

# Sketch-based community detection in evolving networks

Andre Beckus and George K. Atia  
*Department of Electrical and Computer Engineering,  
University of Central Florida, Orlando, FL 32816 USA.*  
(Dated: September 25, 2020)

We consider an approach for community detection in time-varying networks. At its core, this approach maintains a small sketch graph to capture the essential community structure found in each snapshot of the full network. We demonstrate how the sketch can be used to explicitly identify six key community events which typically occur during network evolution: growth, shrinkage, merging, splitting, birth and death. Based on these detection techniques, we formulate a community detection algorithm which can process a network concurrently exhibiting all processes. One advantage afforded by the sketch-based algorithm is the efficient handling of large networks. Whereas detecting events in the full graph may be computationally expensive, the small size of the sketch allows changes to be quickly assessed. A second advantage occurs in networks containing clusters of disproportionate size. The sketch is constructed such that there is equal representation of each cluster, thus reducing the possibility that the small clusters are lost in the estimate. We present a new standardized benchmark based on the stochastic block model which models the addition and deletion of nodes, as well as the birth and death of communities. When coupled with existing benchmarks, this new benchmark provides a comprehensive suite of tests encompassing all six community events. We provide a set of numerical results demonstrating the advantages of our approach both in run time and in the handling of small clusters.

## I. INTRODUCTION

The detection of community structure in networks has garnered a great deal of attention, leading to a vast array of algorithms. Much of the focus has been on static networks, where the goal is to identify groups of nodes within which connections are dense and between which connections are relatively sparse. However, it is often the case that networks evolve with time. For example, edges in social media networks appear and disappear to reflect ever-changing friendships, and gene expression networks continuously evolve in response to external stimuli [1, 2]. In this dynamic setting, new sequential algorithms are needed to track the community structure underlying each temporal snapshot of the network. Here, we propose a sketch-based approach.

Sketching involves the construction of a small synopsis of a full dataset [3]. Notably, this technique has been used in static community detection [4, 5], where a sketch sub-graph is generated by sampling nodes from the full network. The sketch is clustered using an existing community detection algorithm, and the community membership of the nodes in the full network are inferred based on the estimated communities in the sketch. Here, we propose the use of a dynamic sketch which evolves to track the communities in the full network. This dynamic approach addresses two pervasive issues in community detection.

One important concern in community detection is the ability to process large graphs. Many static methods become infeasibly slow when processing a large network, leading to a search for efficient algorithms [6]. The extra time dimension inherent to the dynamic setting only makes this search for efficiency more pressing. However, time-evolving networks also offer a distinct advantage not

found in the static domain. Specifically, evolving networks often possess temporal smoothness in which the community structure changes gradually [7]. In this case, previous snapshots offer prior information which can aid in the clustering of subsequent snapshots. We present a method which relies on a small sketch to convey information regarding previous snapshots. By using a small sketch, the algorithm can detect the main community events without requiring the full graph to be examined, thus reducing the required computational complexity. If the sketch size and number of clusters are fixed, the complexity of our algorithm scales linearly in network size.

Another typical issue found in community detection is the detection of small clusters [8]. If a community shrinks too small, it may become lost, i.e., the community may be absorbed into a larger cluster in the estimated partition. We show that once a cluster is captured in the sketch, it can be tracked even if the cluster becomes very small.

Our algorithm handles the six canonical community events observed in dynamic networks [9]: growth, shrinkage, merging, splitting, birth, and death. The existing benchmarks presented in [10], based on the well-known Stochastic Block Model (SBM) [11], include the first four of these events. Here, we propose a new benchmark which captures the last two events of birth and death. An important feature of the proposed benchmark is that the size of the network varies with time, a characteristic not found in the existing benchmarks. In addition to modeling the birth event, this benchmark incrementally adds new nodes to the network which join existing communities, a feature also not seen in [10]. The benchmarks capture the key fundamental processes under which a network can evolve, and provide a basic foundation for designing a community detection algorithm.

This paper is organized as follows. In Sec. II, we

summarize existing community detection algorithms for evolving networks. Section III describes the network model, summarizes the existing SBM benchmarks, and proposes a new benchmark. In Sec. IV, we describe the sketch-based approach, and formulate techniques by which sketches can track the key evolutionary processes found in the benchmarks. Section V presents the proposed algorithm based on these tracking techniques. We present numerical results in Sec. VI and conclude in Sec. VII.

## II. RELATED WORK: COMMUNITY DETECTION IN EVOLVING NETWORKS

A number of algorithms have been proposed for community detection in evolving networks (see [7, 12] for comprehensive surveys). One straightforward approach entails the independent clustering of each snapshot using a static algorithm. The communities in the current snapshot are matched to the previous communities such that there is continuity in the community identities. This category of algorithm contains a number of variants beginning with the classic work of [13].

More recently, many algorithms take a more sophisticated “dependent” approach, in which previous snapshots are accounted for in the clustering of the current snapshot. These algorithms have the potential to outperform independent community detection algorithms, since they incorporate previous knowledge *directly* in the clustering step.

One approach commonly seen in this category is the representation of each snapshot using a compact graph. In [14], a small weighted graph is constructed after clustering a given snapshot, with each community represented by a single “supernode”. Each supernode’s self loop is weighted to reflect the number of edges within that community, whereas the edge weights between supernodes indicate the number of edges connecting the corresponding communities. When processing the next snapshot, nodes with changed edges are extracted from the supernodes and join the graph as singleton nodes. The graph is then clustered to produce a new partition estimate. In this way, only the first snapshot needs to be clustered in its entirety, with subsequent snapshots being clustered via their compact representation. A similar idea can be seen in dynamic methods built around the static Louvain algorithm [15], for example as seen in [16]. The extension of the Louvain algorithm to time-varying networks follows naturally from its reliance on supernodes. Our approach also uses a small representative graph, however using an altogether different idea of sketching, as described in Sec. IV.

The model used in this paper is based on the SBM [11]. Several recent algorithms have been developed based on dynamic SBM-based models. The dynamic models of [17, 18] specify that nodes move between a fixed set of communities according to a stationary transition proba-

bility matrix. In addition to allowing the movement of nodes between communities, the models of [19–21] also allow the edge probabilities of the communities to vary. Nonetheless, these works focus on the case where individual nodes only change community membership, i.e., the communities undergo the grow and shrink processes.

## III. MODEL DESCRIPTION

Our model follows that described in [10], which is a dynamic extension to the SBM. At time  $t$  the network snapshot is represented by graph  $G(t) = (V(t), E(t))$ , where  $V(t)$  is the set of nodes in existence at time  $t$ , and  $E(t)$  is the set of edges between these nodes. The network is partitioned into at most  $q$  communities. Let  $\mathcal{C}(t) = \{C_\alpha(t) \mid \alpha = 1, \dots, q\}$  be the partition at time  $t$ , with  $C_\alpha(t)$  denoting the set of nodes in community  $\alpha$ . We assume by convention that  $C_\alpha(t) = \emptyset$  if community  $\alpha$  does not exist at time  $t$ . Given a graph  $G = (V, E)$  and node set  $V' \subset V$ , the subgraph of  $G$  induced by  $V'$  is denoted  $G[V']$ .

In each snapshot, an edge exists between nodes within a community with probability  $p_{\text{in}}$ . Unless otherwise specified, nodes in different clusters are connected with probability  $p_{\text{out}}$ . An exception to this rule occurs for the merge-split benchmark, where the intercommunity edge density varies as the community pairs merge and split.

We now describe two existing benchmarks and propose a third benchmark. These benchmarks capture important network processes which we explicitly use in the design of our algorithm.

### A. Existing benchmarks: grow-shrink and merge-split

First, we summarize the existing benchmarks found in [10]. Each benchmark consists of an evolving network containing  $2n$  total nodes. The underlying process is driven by a triangular waveform

$$x(t) = \begin{cases} 2t^*, & 0 \leq t^* < 1/2, \\ 2 - 2t^*, & 1/2 \leq t^* < 1, \end{cases} \quad (1)$$

where

$$t^* \equiv (t/\tau + \phi) \bmod 1, \quad (2)$$

$\tau$  is the period of the waveform, and  $\phi$  controls the phase of the waveform. We will assume that  $\phi = 0$  unless otherwise specified.

The grow-shrink benchmark models the movement of nodes between a pair of communities. At each time step the size of the first community is

$$n_A = n - nf[2x(t + \tau/4) - 1], \quad (3)$$

where the parameter  $f \in [0, 1]$  controls the amount of variation in the sizes of the communities. Since nodes

lost from the first community transfer to the second community, and vice-versa, the size of the second community is  $n_B = 2n - n_A$ . Whenever a node transitions between communities, its edges are regenerated according to the intracommunity and intercommunity edge probabilities  $p_{\text{in}}$  and  $p_{\text{out}}$ , respectively. For  $t \in \{0, \tau/2, \tau\}$  the sizes of the communities are equal. At time  $t = \tau/4$ , a fraction  $f$  of nodes in community A will have moved to community B, whereas at time  $t = 3\tau/4$  the opposite holds.

The merge-split benchmark starts with two communities, each of size  $n$ , with intercommunity edges existing with probability  $p_{\text{out}}$ . New edges are gradually added between the two communities until they are completely merged at time  $t = \tau/2$ , at which point intercommunity edges will exist with probability  $p_{\text{in}}$ . Then, the process reverses and the new edges are removed until the communities are completely split again at time  $t = \tau$ . The snapshots are constructed in the following way. The intracommunity edges are added independently with probability  $p_{\text{in}}$  and remain static throughout the process. The number of intercommunity edges  $m_{\text{um}}$  in the unmerged state are drawn according to a binomial distribution with parameters  $n^2$  and  $p_{\text{out}}$ . The number of edges  $m_{\text{m}}$  in the merged state is similarly drawn, except using probability  $p_{\text{in}}$ . The intercommunity node pairs are sorted in random order, and edges are included between the first

$$m^*(t) = [1 - x(t)]m_{\text{um}} + x(t)m_{\text{m}} \quad (4)$$

node pairs at time  $t$ . In this way, the effective edge density between the two clusters is  $p_{\text{inter}}^* = m^*(t)/n^2$ . The communities are considered merged when

$$p_{\text{in}} - p_{\text{inter}}^* < \sqrt{\frac{1}{n} (p_{\text{in}} + p_{\text{inter}}^*)}. \quad (5)$$

This threshold was chosen based on the community detectability limit found in [22].

The benchmarks are periodic, i.e., the connections in the network at time  $t$  will be exactly identical to those at time  $t + r\tau$ , for any integer  $r$ .

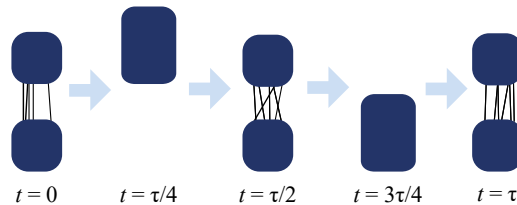
## B. Birth-death benchmark

The grow-shrink and merge-split benchmarks discussed in the previous section lack important features. First, the networks remain fixed in size, with neither new nodes being added to the network, nor existing nodes being removed from the network. Furthermore, they do not model the fundamental processes in which communities are born or die. We now propose a new birth-death benchmark which includes these missing features.

A schematic diagram of the birth-death benchmark is shown in Fig. 1(a). The benchmark consists of two communities which pass into and out of existence. The size of the first community is

$$n_A = \begin{cases} 0, & x(t + \tau/4) \geq 1 - \gamma/2, \\ n[1 - x(t + \tau/4)], & \text{otherwise,} \end{cases} \quad (6)$$

(a) Birth-Death benchmark



(b) Mixed (three benchmarks)

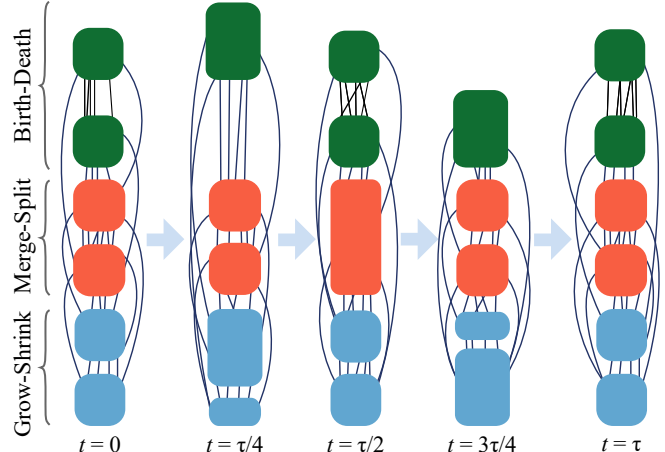


FIG. 1. (a) Schematic representation of the birth-death benchmark. (b) Schematic representation of the mixed benchmark which stacks the grow-shrink, merge-split, and birth-death benchmarks.

where the parameter  $\gamma \in [0, 1]$  controls the minimum size of the community. When  $n_A = 0$ , the community is non-existent. The community starts at time  $t = 0$  with  $n/2$  nodes. These nodes are removed from the community, and deleted from the network, until the community shrinks to size  $\gamma n/2$  at time  $t = \tau(1 - \gamma)/4$ . At this point, the community dies and all of its remaining nodes are deleted from the network. At time  $t = \tau(1 + \gamma)/4$ , a new set of  $\gamma n/2$  nodes is added to the network and used to recreate the community. New nodes are gradually created and added to the community until it reaches size  $n$ . At this point, nodes are again removed from the community until it contains  $n/2$  nodes, and the process repeats.

The second community is of size

$$n_B = \begin{cases} 0, & x(t + \tau/4) < \gamma/2 \\ n x(t + \tau/4), & \text{otherwise.} \end{cases} \quad (7)$$

This community undergoes essentially the same process as the first community except with a phase shift of  $\tau/2$ .

We note that the birth-death benchmark includes elements of the grow-shrink process, in the sense that nodes are added to and removed from the communities in the intervening time between the birth and death events. However, in contradistinction to the grow-shrink benchmark, the nodes joining the communities are newly created, as opposed to *existing* nodes moved from one community to the other. Similarly, nodes removed from a community

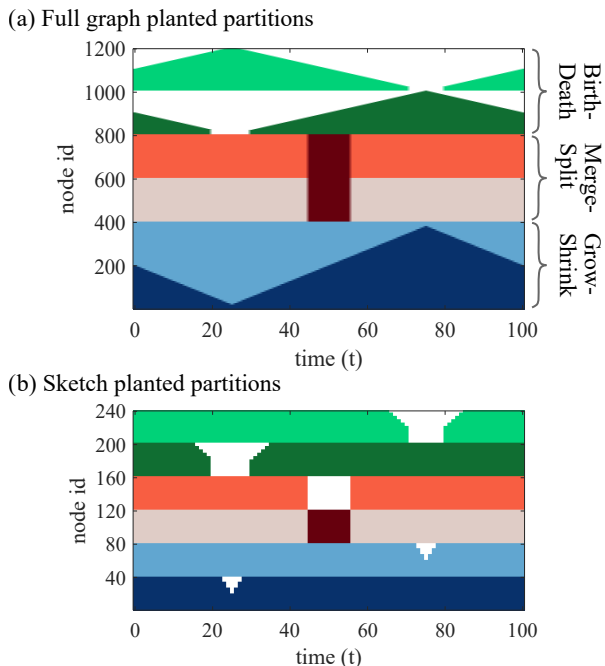


FIG. 2. (a) Planted partitions for full graphs. Each vertical slice indicates the planted partition at time  $t$ . (b) Sketches produced with  $n' = 40$ . Each vertical slice indicates the planted partitions in sketch  $\mathcal{S}(t)$ . White regions indicate that the corresponding node does not exist at time  $t$ .

are deleted from the network rather than transferred to the other community.

### C. Mixed (three benchmarks)

In [10], a mixed benchmark is created by “stacking” the grow-shrink and merge-split benchmarks such that there are  $4n$  nodes containing four communities. Two of the clusters, together containing  $2n$  nodes, undergo the grow-shrink process while the other two clusters, also containing  $2n$  nodes, undergo the merge-split process.

We propose an extended mixed benchmark to include the birth-death benchmark. A schematic of this mixed benchmark is shown in Fig. 1(b). The benchmark has a maximum of  $6n$  nodes. The first  $4n$  nodes contain the grow-shrink and merge-split benchmarks as previously described, whereas the last  $2n$  nodes participate in the birth-death process (the actual number of nodes varies with time due to addition and deletion of nodes in the birth-death benchmark). We show an example of this mixed benchmark in Fig. 2(a), having parameters  $n = 200$ ,  $q = 6$ ,  $f = 0.9$ ,  $\gamma = 0.2$ .

## IV. SKETCH-BASED TRACKING OF DYNAMIC PROCESSES

Our algorithm relies on a small representative sketch of the full network. The sketch captures important information which can be used to track the processes by which the network evolves. Meanwhile, the smaller size of the sketch allows these checks to be performed quickly without requiring a complete assessment of the entire network.

We first describe the sketch in detail, and then describe how this sketch can be used to detect specific events in each of the fundamental processes described in Sec. III. For the sake of clarity, we will consider the detection of each process in isolation, and in Sec. V present an algorithm which exploits all three techniques to track concurrent processes occurring in the same network.

### A. Dynamic sketching

The sketch consists of a set of nodes sampled from the full network. At each time step, this set is updated to reflect the current state of the full network. The set of nodes in the sketch at time  $t$  is denoted  $\mathcal{S}(t)$ , and the subset of these nodes from cluster  $\alpha$  is denoted  $C'_\alpha(t) = \mathcal{S}(t) \cap C_\alpha(t)$ .

The sketch-based approach allows flexibility to choose which nodes are placed in the sketch. For the SBM used here – in which the intracommunity edges are placed with the same probability  $p_{\text{in}}$  for all communities – algorithms generally have better success rates when the communities are of equal size [5]. In our approach, rather than requiring that the full network be balanced, we can instead improve the possibility of success by maintaining a balanced sketch. Ideally, all clusters in the sketch should be of equal size  $n'$ , but since communities in the full network may be smaller than  $n'$ , we set the size of community  $C'_\alpha(t)$  as

$$\min\{n', |C_\alpha(t)|\}. \quad (8)$$

An example sketch time series is shown in Fig. 2(b), where nodes have been sampled from the mixed benchmark shown in Fig. 2(a) according to (8). For the grow-shrink and birth-death processes, the white space indicates non-existent nodes, i.e., where the community sizes are smaller than  $n'$ .

For this example, we build the sketches using knowledge of the planted community partitions. The proposed algorithm has no such knowledge, and therefore must build the sketches based on its community estimates. We will present an actual set of sketch produced by the proposed algorithm in Sec. VID.

## B. Merge-split process

Suppose that we have a cluster  $\alpha$  which is undergoing a split into two separate communities. We propose detection of the emerging clusters by using spectral techniques – here we use a simple approach based on the spectral gap heuristic [23].

First, we consider how to obtain the spectral gap in the current snapshot  $G(t)$  based on the last estimate of the splitting community  $C_\alpha(t-1)$ . Let  $\mathbf{A}$  be the adjacency matrix of the subgraph of  $G(t)$  induced by  $C_\alpha(t-1)$ . If  $\mathbf{D}$  is the diagonal matrix containing the degrees of the nodes in  $\mathbf{A}$  along the diagonal, then the normalized graph Laplacian is defined as [24]

$$\mathbf{L} = \mathbf{I} - \mathbf{D}^{-1/2} \mathbf{A} \mathbf{D}^{-1/2}. \quad (9)$$

Let  $\lambda_1, \lambda_2, \lambda_3$  be the three smallest eigenvalues of  $\mathbf{L}$  in increasing order. The eigengap heuristic states that if there is one community,  $\lambda_2 - \lambda_1$  will tend to be large, whereas if there are two communities present, then  $\lambda_2 - \lambda_1$  will tend to be smaller than  $\lambda_3 - \lambda_2$ . Noting that  $\lambda_1 = 0$ , we can determine the state of the process by monitoring

$$\lambda_{\text{gap}} = (\lambda_3 - \lambda_2) / \lambda_3. \quad (10)$$

An example is shown in Fig. 3 for a network having parameters  $q = 2, n = 200, p_{\text{in}} = 0.5, p_{\text{out}} = 0.05$ . The planted partitions are shown in Fig. 3(a), and the dashed blue line in Fig. 3(b) shows the corresponding value of  $\lambda_{\text{gap}}$  for each time step. As can be seen, the value of  $\lambda_{\text{gap}}$  increases as the process moves in either direction away from the fully merged state (at  $t = 50$ ) and towards the fully split state (at  $t \in \{0, \tau\}$ ). For reference, the detectability limit that formally defines the split in the benchmark is shown as a vertical dashed line.

Rather than finding the eigenvalues for the community in the full network, we propose to estimate  $\lambda_{\text{gap}}$  based on the sketch. We use the same procedure as described above, but instead let  $\mathbf{A}$  be the adjacency matrix of the subgraph of  $G(t)$  induced by  $C'_\alpha(t-1)$  rather than  $C_\alpha(t-1)$ . This estimate is shown in Fig. 3(b) as a solid orange line. Here, we use an ideal sketch as described in Sec. IV A, with the sketch constructed using  $n' = 50$  nodes sampled uniformly at random from each community at each time step. We note that the estimated value tends to be smaller than the actual value, thus making the split harder to detect. This is consistent with the fact that the sketch detectability limit – shown as a vertical dotted line – is larger due to the smaller cluster sizes (note that the right hand side of (5) is inversely proportional to cluster size). Nonetheless, the estimate still allows the split to be identified. If more precision is required, a two-stage process could be used in which a small value in the estimate triggers a calculation of the exact value  $\lambda_{\text{gap}}$  at a higher computational expense. Section V will discuss how the new partition is estimated once the split event is detected.

For the merge process, we exploit the fact that the two communities are already known at time  $t-1$ . This

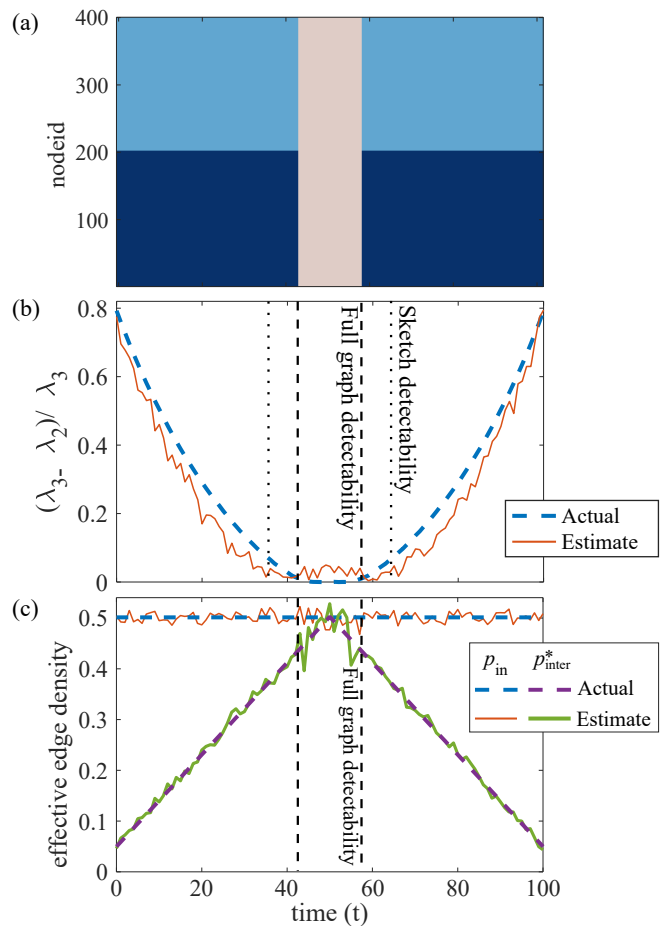


FIG. 3. (a) Planted partitions of the merge-split benchmark. (b) Actual and estimated value of  $\lambda_{\text{gap}}$  at each time step. (c) Actual and estimated value of  $p_{\text{in}}, p_{\text{inter}}^*$  at each time step.

means that we can estimate  $p_{\text{in}}$  and  $p_{\text{inter}}^*$  and use these estimates to directly check condition (5). Suppose that communities  $\alpha, \alpha'$  are merging. The sketch allows us to quickly calculate empirical estimates of the edge probabilities using the expressions

$$\hat{p}_{\text{in}} = \sum_{u \in \{1, \dots, q\}} \frac{2 |\{ (i, j) \in E(t) \mid j \in C'_u(t-1) \}|}{|C'_u(t-1)|^2}, \quad (11)$$

$$\hat{p}_{\alpha, \alpha'} = \frac{|\{ (i, j) \in E \mid i \in C'_\alpha(t-1), j \in C'_{\alpha'}(t-1) \}|}{|C'_\alpha(t-1)| |C'_{\alpha'}(t-1)|}. \quad (12)$$

Figure 3(c) shows the actual (dashed blue line) and estimated (solid orange line) values of  $p_{\text{in}}$  for the example in Fig. 3(a). The actual (dashed purple line) and estimated (solid green line) values of  $p_{\text{inter}}^*$  are also shown in the sample plot. In both cases, the estimates track the actual values well.

### C. Birth-death process

First, we consider how to handle the incremental addition of new nodes to the network when these new nodes join an existing cluster. Suppose that at time  $t$  a set of nodes  $V^+(t)$  is added to community  $\alpha$ . We can estimate the correct community for a new node  $i \in V^+(t)$  by evaluating its connectivity to the existing nodes in each cluster. To this end, we define

$$s_{i,u}(t) = \frac{|\{(i, j) \in E(t) \mid j \in C'_u(t-1)\}|}{|C'_u(t-1)|}, \quad (13)$$

where it is assumed that  $s_{i,u}(t) = 0$  if  $C'_u(t-1)$  is empty. Noting that

$$\mathbb{E}[s_{i,u}(t)] = \begin{cases} p_{\text{in}}, & u = \alpha, \\ p_{\text{out}}, & u \neq \alpha, \end{cases} \quad (14)$$

we can see that  $s_{i,u}(t)$  serves as a point estimate of the probability that there is an edge between node  $i$  and an arbitrary node in  $C'_u(t-1)$ . Node  $i$  can then be assigned to the cluster  $\alpha$  with which connectivity is greatest, i.e., where

$$\alpha = \arg \max_{u \in \{1, \dots, q\}} s_{i,u}(t). \quad (15)$$

The variance in  $s_{i,u}(t)$  is

$$\text{Var}(s_{i,u}(t)) = \begin{cases} \frac{p_{\text{in}}(1-p_{\text{in}})}{|C'_u(t-1)|}, & u = \alpha, \\ \frac{p_{\text{out}}(1-p_{\text{out}})}{|C'_u(t-1)|}, & u \neq \alpha. \end{cases} \quad (16)$$

While the expected value is independent of sketch cluster size, the variance grows as the clusters shrink, thus motivating the use of equal-sized communities.

Now, consider the birth event in which some or all of the nodes  $V^+(t)$  are added to a new community which does not exist at time  $t-1$ . In this case, the expectation  $\mathbb{E}[s_{i,u}(t)]$  will equal  $p_{\text{out}}$  for *any* existing cluster. We can therefore identify these nodes as those having a connectivity significantly below the intracommunity density estimate found in (11). For determining an exact threshold, the standard deviation of the intracommunity density can be estimated as

$$\hat{\sigma}_{p_{\text{in}}} = \sqrt{\frac{2\hat{p}_{\text{in}}(1-\hat{p}_{\text{in}})}{\sum_{u \in \{1, \dots, q\}} |C'_u(t-1)|^2}}. \quad (17)$$

We then define the set of nodes in new clusters as

$$V_{\text{birth}} = \{i \in V^+(t) \mid s_{i,u}(t) < \hat{p}_{\text{in}} - 3\hat{\sigma}_{p_{\text{in}}}, \forall u \in \{1, \dots, q\}\} \quad (18)$$

Since it is possible that the new nodes belong to multiple new clusters, we apply the static clustering algorithm found in [5] to cluster  $V_{\text{birth}}$  (see Sec. V for details). When nodes are deleted, the algorithm needs to remove these deleted nodes from the sketch, and then replace them by selecting new nodes from the same community uniformly at random.

### D. Grow-shrink process

Suppose that two clusters are evolving under the grow-shrink process, and that at time  $t$ , a set of nodes  $V_{\alpha \rightarrow \alpha'}$  moves from cluster  $\alpha$  to cluster  $\alpha'$ . To identify these nodes, we propose to use  $s_{i,u}(t)$ . The number of nodes in  $V_{\alpha \rightarrow \alpha'}$  that are also contained in the sketch is

$$m' = |V_{\alpha \rightarrow \alpha'} \cap \mathcal{S}(t-1)|. \quad (19)$$

For a node  $i$  in community  $\alpha$ , we have for an arbitrary community  $u$ ,

$$\mathbb{E}[s_{i,u}(t)] = \begin{cases} p_{\text{in}} - \frac{m'(p_{\text{in}} - p_{\text{out}})}{|C'_u(t-1)|}, & u = \alpha, \\ p_{\text{out}}, & u = \alpha', \end{cases} \quad (20)$$

while for a node  $j$  in community  $\alpha'$  we have

$$\mathbb{E}[s_{j,u}(t)] = \begin{cases} p_{\text{in}}, & u = \alpha', \\ p_{\text{out}} + \frac{m'(p_{\text{in}} - p_{\text{out}})}{|C'_u(t-1)|}, & u = \alpha. \end{cases} \quad (21)$$

For either node, the gap between the expected similarities for the correct and incorrect communities is

$$\begin{aligned} & \mathbb{E}[s_{i,\alpha}(t)] - \mathbb{E}[s_{i,\alpha'}(t)] \\ &= \mathbb{E}[s_{j,\alpha'}(t)] - \mathbb{E}[s_{j,\alpha}(t)] \\ &= (p_{\text{in}} - p_{\text{out}}) \left[ 1 - \frac{m'(p_{\text{in}} - p_{\text{out}})}{|C'_\alpha(t-1)|} \right]. \end{aligned} \quad (22)$$

If the sketch size is set such that  $|C'_\alpha(t-1)| \gg m'(p_{\text{in}} - p_{\text{out}})$ , then the reliability of (15) will be driven primarily by the density gap  $p_{\text{in}} - p_{\text{out}}$ .

## V. ALGORITHM

We first describe two procedures upon which the algorithm depends, and then present the proposed algorithm itself. We finish with an analysis of the computational complexity of this algorithm.

### A. Preliminaries

In order to cluster the first snapshot, and to partition new and splitting communities, we invoke the static sketch-based community detection framework found in [4, 5]. This framework first produces a static sketch of the full graph  $G$  using the *SamPLing Inversely proportional to Node degree* (SPIN) method [5], as detailed in the following procedure.

#### Sample-SPIN( $G, N'$ )

- (1)  $P_i \leftarrow \left( d_i \sum_{j \in V} d_j^{-1} \right)^{-1}$  for  $i = 1, \dots, |V|$ .
- (2) Sample  $N'$  nodes without replacement to form set  $\mathcal{S}$ . Node  $i$  should be sampled with probability  $P_i$ .
- (3) **return**  $\mathcal{S}$

Next, the framework applies an existing community detection algorithm  $\mathcal{A}$  to the sketch  $\mathcal{S}$ , and the membership of the nodes in the full graph are inferred based on the estimated partition. These steps are captured in the following procedure.

**Static-Cluster**( $G, \mathcal{S}$ )

- (1)  $G' \leftarrow G[\mathcal{S}]$
- (2) Invoke community detection algorithm  $\mathcal{A}$  on  $G'$  to get sketch partition estimate  $C' = \{C'_1, \dots, C'_{\hat{q}}\}$ , where  $\hat{q}$  is the estimated number of clusters.
- (3)  $C_u \leftarrow \emptyset$  for  $u = 1, \dots, \hat{q}$
- (4) **for** each node  $i \in V$  **do**
- (5)  $\alpha \leftarrow \arg \max_{u \in \{1, \dots, \hat{q}\}} \frac{|\{(i, j) \in E \mid j \in C'_u\}|}{|C'_u|}$
- (6)  $C_\alpha \leftarrow C_\alpha \cup \{i\}$
- (7) **end for**
- (8) **return** partition  $\mathcal{C} = \{C_\alpha \mid \alpha = 1, \dots, \hat{q}\}$

This static community detection framework has two key advantages. First, applying algorithm  $\mathcal{A}$  to a small sketch reduces the computational complexity of this costly step as compared to clustering the full graph. Second, when  $G$  contains communities of disproportionate size, the SPIN tends to produce a sketch with more uniform community sizes, thus improving the likelihood of success in the subsequent clustering step.

## B. Proposed algorithm

We now present the proposed algorithm, followed by a description of its steps.

Input: Sketch community size  $n'$ . Graph snapshots  $G(t), t = 0, 1, \dots$

- (1)  $\mathcal{S}' \leftarrow \mathbf{Sample-SPIN}(G(0), qn')$
- (2)  $\mathcal{C}(0) \leftarrow \mathbf{Static-Cluster}(G(0), \mathcal{S}')$
- (3) Build sketch  $\mathcal{S}(0)$  by sampling  $n'$  nodes uniformly at random from each community  $C \in \mathcal{C}(0)$ . If  $n' > |C|$ , then include all nodes from  $C$ .
- (4)  $r \leftarrow |\mathcal{C}(0)|$ .
- (5) **for**  $t = 1, 2, \dots$  **do**
- (6)  $G \leftarrow G(t)$
- (7)  $C_u \leftarrow \emptyset$  for  $u \in \{1, \dots, r\}$
- (8) Build set  $V_{\text{birth}}$  using equation (18).
- (9) **if**  $V_{\text{birth}} \neq \emptyset$  **then**
- (10)  $\bar{G} \leftarrow G[V_{\text{birth}}]$
- (11)  $\bar{\mathcal{S}} \leftarrow \mathbf{Sample-SPIN}(\bar{G}, n')$
- (12)  $\{C_{r+1}, \dots, C_{r+\hat{q}}\} \leftarrow \mathbf{Static-Cluster}(\bar{G}, \bar{\mathcal{S}})$
- (13)  $r \leftarrow r + \hat{q}$
- (14) **end if**
- (15) **for** each node  $i \in V(t) \setminus V_{\text{birth}}$  **do**
- (16)  $\alpha \leftarrow \arg \max_{u \in \{1, \dots, r\}} s_{i,u}(t)$
- (17)  $C_\alpha \leftarrow C_\alpha \cup \{i\}$
- (18) **end for**
- (19) **for**  $\alpha \in \{1, \dots, r\}$ , where  $|C_\alpha| > a$  **do**
- (20)  $C' \leftarrow C_\alpha \cap \mathcal{S}(t-1)$

$$(21) \quad G' \leftarrow G[C']$$

(22) Let  $\mathbf{A}$  be the adjacency matrix of  $G'$ . Calculate eigenvalues  $\lambda_2, \lambda_3$  of the normalized Laplacian  $\mathbf{L}$  defined in equation (9) (see Sec. IV B). Calculate  $\lambda_{\text{gap}}$  as in equation (10).

- (23) **if**  $\lambda_{\text{gap}} > b$  **then**
- (24)  $G_\alpha \leftarrow G[C_\alpha]$
- (25)  $\{C_\alpha, C_{r+1}\} \leftarrow \mathbf{Static-Cluster}(G_\alpha, C')$
- (26)  $r \leftarrow r + 1$
- (27) **end if**
- (28) **end for**
- (29) **for** community pairs  $\alpha, \alpha' \in \{1, \dots, r\}$  **do**
- (30) **if**  $\hat{p}_{\text{in}} - \hat{p}_{\alpha, \alpha'} < c \sqrt{\frac{2(\hat{p}_{\text{in}} + \hat{p}_{\alpha, \alpha'})}{|C_\alpha| + |C_{\alpha'}|}}$  **then**
- (31)  $C_\alpha \leftarrow C_\alpha \cup C_{\alpha'}$
- (32)  $C_{\alpha'} \leftarrow \emptyset$
- (33) **end if**
- (34) **end for**
- (35)  $\mathcal{C}(t) \leftarrow \{C_u \mid u = 1, \dots, r\}$
- (36)  $\mathcal{S}(t) \leftarrow \mathcal{S}(t-1) \setminus V^-$
- (37) Re-proportion sketch  $\mathcal{S}(t)$  such that it contains  $\min\{n', |C|\}$  nodes from each community  $C \in \mathcal{C}(t)$ .

(38) **end for**

Output: Partitions  $\mathcal{C}(t), t = 0, 1, \dots$

Steps 1-2 cluster the first graph snapshot. This first partition estimate is used to construct a balanced sketch in step 3. The remainder of the algorithm processes each subsequent snapshot, handling each of the processes described in Sec. IV.

First, the grow-shrink and birth-death processes are addressed. Steps 8-14 identify and partition the set of newly-born communities. Meanwhile, steps 15-18 re-evaluate the community membership of existing nodes, as well as new nodes joining existing communities, i.e., new nodes not in  $V_{\text{birth}}$ . We note that the algorithm re-evaluates all nodes for simplicity, but we could reduce the time required for this step by only re-evaluating nodes with changed edges.

Steps 19-28 handle splits within each community. Only communities with size greater than  $a$  are checked, as the spectral estimates become unreliable for small communities. If the spectral gap  $\lambda_{\text{gap}}$  exceeds threshold parameter  $b$ , then a split is declared and step 25 bi-partitions the community. If the community is undergoing a split into more than two communities, then the additional communities will be detected and split at the next time step, a sequence which is reminiscent of the recursive bi-partitioning scheme sometimes used in spectral clustering [25]. Parameters  $a$  and  $b$  can be determined based on the merge-split benchmark as shown in Fig. 3. First, we can find the smallest value of  $n'$  which gives a sufficiently reliable estimate of  $\lambda_{\text{gap}}$ , and then set  $a$  to this value. Second, the parameter  $b$  should be set high enough such that noise in the estimate of  $\lambda_{\text{gap}}$  during the merged state will not prematurely trigger a split (when  $n'$  is set as specified in the input to the algorithm). In this paper,

we set  $a=20, b=0.1$ .

Finally, steps 29-34 handle pairs of communities which merge. Step 30 checks a condition similar to equation (5), except with  $n$  set to the average of the community sizes, and an additional scaling parameter  $c$  in the right hand side. It might seem best to set  $c=1$  such that it exactly matches the detectability threshold in equation (5). However, the shrinking density gap  $\widehat{p}_{\text{in}} - \widehat{p}_{\alpha, \alpha'}$  causes erratic behavior in step 16, resulting in nodes incorrectly being moved between the pair of merging communities. This in turn corrupts the estimates  $\widehat{p}_{\text{in}}, \widehat{p}_{\alpha, \alpha'}$ . We find that triggering the merge earlier by setting  $c=2$  avoids this issue.

### C. Computational complexity analysis

In this section, we take  $q$  to be the maximum number of communities, and  $N$  to be the maximum number of nodes in any given snapshot. For the proposed algorithm, the complexity for estimating each partition  $\mathcal{C}(t), t \geq 0$  is  $\mathcal{O}(q^2 n' (qn'^2 + N))$ . A detailed justification for this result follows.

We start by commenting on the complexity of the procedures in Sec. V A. The computational complexity of **Sample-SPIN** is  $\mathcal{O}(N' |V|)$ . The complexity of **Static-Cluster** depends on which algorithm  $\mathcal{A}$  is chosen. We assume  $\mathcal{A}$  to be at most cubic in  $|\mathcal{S}|$ , whereas steps 4-7 of **Static-Cluster** incur a cost of  $\mathcal{O}(\hat{q} |\mathcal{S}| |V|)$  time. Therefore, the run time of this procedure is  $\mathcal{O}(|\mathcal{S}| (|\mathcal{S}|^2 + \hat{q} |V|))$ .

The proposed algorithm first estimates the communities  $\mathcal{C}(0)$  in  $G(0)$ . Since  $|\mathcal{S}| = qn'$ , step 1 takes  $\mathcal{O}(q^2 n'^3)$  time, and step 2 takes  $\mathcal{O}(q^2 n' (qn'^2 + N))$  time. We now consider the remainder of the algorithm, which estimates the community partitions  $\mathcal{C}(t)$  in each snapshot  $G(t)$  for  $t > 0$ . Steps 8-14 take  $\mathcal{O}(q^2 n' (qn'^2 + N))$  time due to the cost of invoking **Sample-SPIN** and **Static-Cluster**. Calculation of the similarity metric  $s_{i,u}(t)$  for a single community  $u$  and single node  $i$  takes time  $\mathcal{O}(n')$ , and so steps 15-18 take time  $\mathcal{O}(qn'N)$  in total. For the split detection, calculation of the eigenvalues in step 22 takes  $\mathcal{O}(n'^3)$  time. If a split is detected, then the bi-partitioning in step 25 takes  $\mathcal{O}(n'(n'^2 + N))$  time, since the size of the sketch  $C'$  is  $\mathcal{O}(n')$ . The aforementioned steps are repeated for each community, and so steps 19-28 altogether run in  $\mathcal{O}(qn'^3)$  time. For the merge detection, the estimates  $\widehat{p}_{\text{in}}$  and  $\widehat{p}_{\alpha, \alpha'}$  (for all community pairs  $\alpha, \alpha'$ ) can be calculated once per snapshot at a total cost of  $\mathcal{O}(n'^2)$ . Once these estimates are calculated, the loop in steps 29-34 runs in  $\mathcal{O}(q^2)$  time. In conclusion, the run time for the first snapshot in steps 1-3, and for each subsequent loop of steps 6-37, are both  $\mathcal{O}(q^2 n' (qn'^2 + N))$ . This yields the stated result.

## VI. RESULTS

We now present results demonstrating the performance of the proposed algorithm. For comparison, results are also shown for four different algorithms. First, we use a classic “independent” community detection approach based on those described in [13, 26]. This approach applies a community detection algorithm  $\mathcal{A}$  to each snapshot to obtain community estimates  $\mathcal{C} = \{C_1, \dots, C_q\}$ . To provide continuity in the community assignments of the nodes, community  $i$  in the each snapshot at time  $t > 0$  is matched to the community at time  $t-1$  having the largest overlap. To measure overlap, we use the Jaccard coefficient [27]. Specifically, for each community  $\alpha$ , we set  $C_\alpha(t) = C_{\alpha'}$  where

$$\alpha' = \arg \max_u \frac{|C_\alpha \cap C_u(t-1)|}{|C_\alpha \cup C_u(t-1)|}. \quad (23)$$

This algorithm is referred to as Standard Independent (SI). Second, we apply a variation of SI, in which the static sketch-based algorithm of [5] is applied to each snapshot, using sketch size  $N' = n'q$ . The sketch-based algorithm uses an arbitrary algorithm  $\mathcal{A}$  to partition the sketch. We refer to this method as Sketch-based Independent (SbI). Third, we run the algorithm of [14], which we refer to here as (Dinh, 2009). Lastly, we use ESPRA (*Evolutionary clustering based on Structural Perturbation and Resource Allocation similarity*), which is based on structural perturbation theory [28]. When running the ESPRA algorithm, we use the same parameters as used in the experimental results of [28]:  $\alpha = 0.8, \beta = 0.5$ .

All of the algorithms, with the exception of ESPRA, can invoke an arbitrary community detection algorithm  $\mathcal{A}$ . Here, we use spectral clustering [24], and estimate the number of communities using the eigengap heuristic [23]. Specifically, let  $\mathbf{A}$  be the adjacency matrix of the entire graph snapshot, and let  $\lambda_1, \dots, \lambda_q$  be the  $q$  smallest eigenvalues of the Laplacian  $\mathbf{L}$  defined in (9). Then the estimated number of clusters is

$$\widehat{q} = \arg \max_{r \in \{q^-, \dots, q\}} (\lambda_{r+1} - \lambda_r), \quad (24)$$

where  $q^-$  is the minimum number of possible clusters. The communities are identified by performing k-means clustering on the first  $\widehat{q}$  eigenvectors of  $\mathbf{L}$ .

We note that SI and SbI cannot handle the birth and split processes, and therefore we only apply these algorithms to the grow-shrink benchmark. Furthermore, ESPRA does not account for networks of changing size, and therefore is only applied to the grow-shrink and merge-split benchmarks. Both the proposed algorithm and (Dinh, 2009) can accommodate all of the benchmarks.

First, we show the run time of the proposed algorithm. Second, we demonstrate the ability of the algorithm to handle small clusters in the birth-death and grow-shrink benchmarks. Next, we demonstrate the performance of the algorithm on the merge-split benchmark, as well as

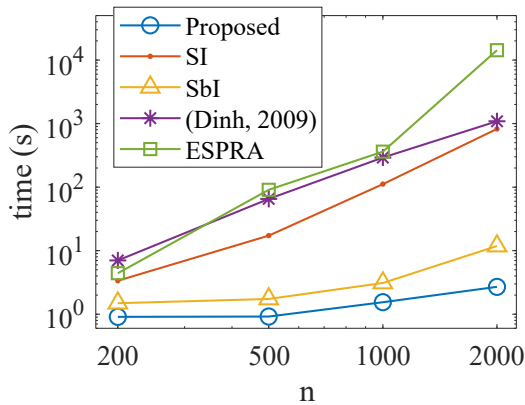


FIG. 4. Timings results for the algorithms on the grow-shrink benchmark. Time is averaged over 10 trials and plot using logarithmic scales for both axes.

on the mixed benchmark. Finally, we perform a sensitivity analysis showing how varying sketch size affects the success rate of the algorithm.

### A. Run time

We first demonstrate the speed-ups possible with the proposed algorithm. We run all of the algorithms on the grow-shrink benchmark with parameters  $q = 2$ ,  $n' = 100$ ,  $p_{\text{in}} = 0.5$ ,  $p_{\text{out}} = 0.05$ ,  $f = 0.5$ , and show the results in Fig. 4. All algorithms had perfect community estimates for all network sizes, except for ESPRA which still performed well, with less than 0.02% of the nodes being misclassified (on average) in every snapshot. The proposed algorithm finishes very fast, in under three seconds for all cases. SbI also rapidly clusters the network time-series through its use of sketching. While both SbI and the proposed algorithm scale well with increasing network size, the proposed algorithm still holds an advantage in success rate given that it carries over the sketch from previous iterations (we will show an example of this in the next section). Both SI and ESPRA apply spectral techniques to the full graph, and therefore scale super-linearly with network size. Although (Dinh, 2009) clusters a graph of reduced size at each time step, nodes having changed edges are left as singleton nodes. In this example, the edge changes are sufficient to keep many nodes as singletons, thus increasing the graph size and run time.

### B. Performance with small clusters

We now use the grow-shrink and birth-death benchmarks to evaluate the algorithms' handling of small clusters. We use normalized agreement to compare the planted communities  $\mathcal{C} = \{C_1, \dots, C_q\}$  and estimated communities  $\hat{\mathcal{C}} = \{\hat{C}_1, \dots, \hat{C}_q\}$  (empty communities are

added to the smaller set such that  $|\mathcal{C}| = |\hat{\mathcal{C}}|$ ). Normalized agreement is defined as [29]

$$\tilde{A} = \frac{1}{q} \max_{\pi} \sum_{\substack{u=1 \\ |C_u| > 0}}^q \frac{|C_u \cap \hat{C}_{\pi(u)}|}{|C_u|}, \quad (25)$$

where  $\pi$  ranges over the permutations on  $q$  elements (this permutation is necessary since the community indices may be ordered arbitrarily). Normalized agreement proves useful for quantifying performance in the presence of small clusters, since each community constitutes a fraction  $1/q$  of the normalized agreement, regardless of community size. The normalized agreement for the snapshot at time  $t$  is denoted  $\tilde{A}(t)$ . Plots of  $\tilde{A}(t)$  show an ensemble average over 50 independent runs.

For summarizing the overall deviation in the actual and estimate communities for a snapshot sequence, we use the average-squared error

$$E_{\tilde{A}} = \frac{1}{T} \sum_{t=1}^T [1 - \tilde{A}(t)]^2, \quad (26)$$

where  $T$  is the total number of snapshots. When plotting  $E_{\tilde{A}}$ , we take an average over 50 independent trials.

We first consider a network with two concurrent instances of the birth-death benchmark. For the first instance, we set  $n = n_1$  and use a phase shift of  $\phi = 0$ , whereas for the second instance we set  $n = 500 - n_1$  and use a phase shift of  $\phi = \tau/2$ . Both instances have parameters  $q = 4$ ,  $p_{\text{in}} = 0.5$ ,  $p_{\text{out}} = 0.05$ ,  $q^- = 2$ . We set  $n' = 50$ , which leads to a maximum sketch size of 200 nodes.

One means for producing small clusters is by using small values of  $\gamma$ , such that each community is small immediately after birth and before death. An example is shown in Fig. 5(a), with  $\gamma = 0.1$  and  $n_1 = 250$ . The community detection results are shown in Fig. 5(b) using both the proposed algorithm and (Dinh, 2009). The algorithm of (Dinh, 2009) tends to absorb the small communities into the large communities, as exhibited by the large drop in normalized agreement immediately after birth and before death. Meanwhile, the proposed algorithm maintains  $\tilde{A}(t) > 0.998$  for all  $t \geq 0$ . We expand on this example by plotting  $E_{\tilde{A}}$  as a function of  $\gamma$  in Fig. 5(c). As with the previous example, we have balanced instance sizes with  $n_1 = 250$ . The proposed algorithm has  $E_{\tilde{A}} < 0.002$  for all values of  $\gamma$ .

Another means for introducing small clusters is by reducing  $n_1$ , i.e., making smaller communities in the first benchmark instance while at the same time increasing the sizes of the communities in the second instance. For this example, we use a smaller sketch size with  $n' = 25$ . The value of  $E_{\tilde{A}}$  is shown in Fig. 5(d) for varying  $n_1$  with  $\gamma = 0.5$ . For the proposed algorithm,  $E_{\tilde{A}}$  remains below 0.005 for  $n_1 \geq 40$ . On the other hand, (Dinh, 2009) does not fall under this threshold until  $n_1 \geq 100$ .

We now present analogous examples for the grow-shrink benchmark. There are two instances of the grow-shrink benchmark with parameters  $\phi = 0$ ,  $n = n_1$  for the

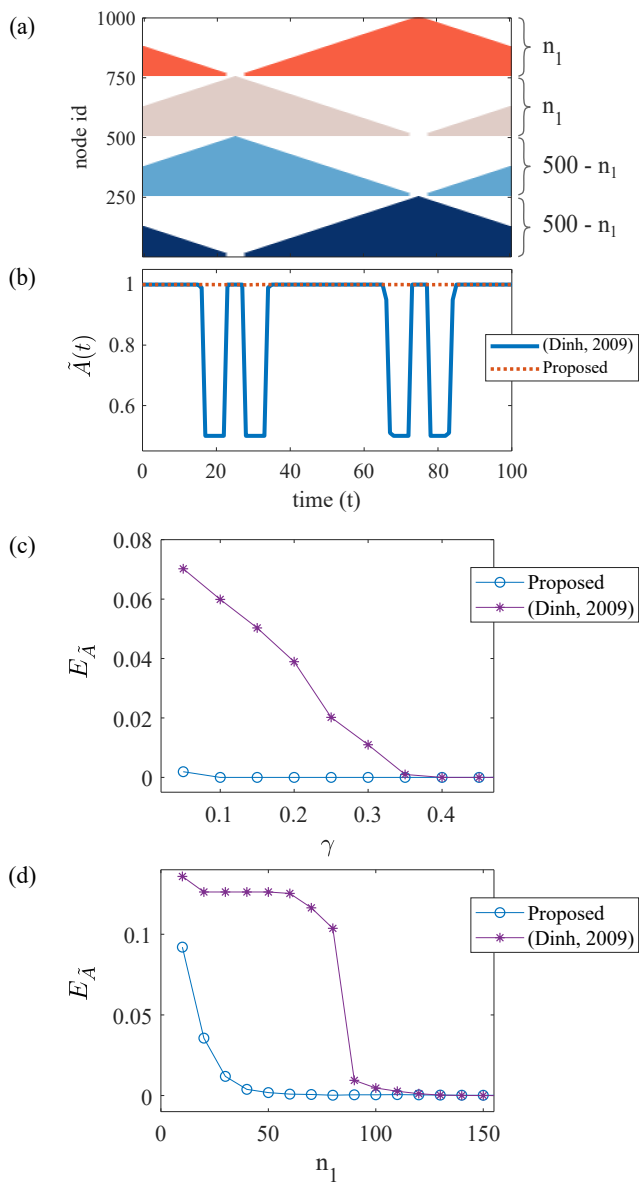


FIG. 5. (a) Planted partitions for a double-stacked version of the birth-death benchmark, with  $n_1 = 250$ ,  $\gamma = 0.1$ . (b) Normalized agreement  $\tilde{A}(t)$  plot as a function of time. Squared error of normalized agreement  $E_{\tilde{A}}$  is shown for (c) varying  $\gamma$  with  $n_1 = 250$  and (d) varying  $n_1$  with  $\gamma = 0.5$ .

first instance, and  $\phi = \tau/2$ ,  $n = 500 - n_1$  for the second instance. Figure 6(a) shows planted partitions for an example with  $f = 0.95$ . For the proposed algorithm we set  $n' = 50$ , and for SbI, we use a sketch size of 200 (to match the sketch size used in the proposed algorithm).

As with the birth-death benchmark, we can produce smaller clusters by reducing the value of  $n_1$ . Results are shown in Fig. 6(b) for varying  $n_1$ . We can also produce small communities by increasing  $f$ . This makes two small communities and two large communities at both  $t = \tau/4$  and  $t = 3\tau/4$ . The value of  $E_{\tilde{A}}$  is shown as a function of  $f$  in Fig. 7(a). Both the proposed algorithm and

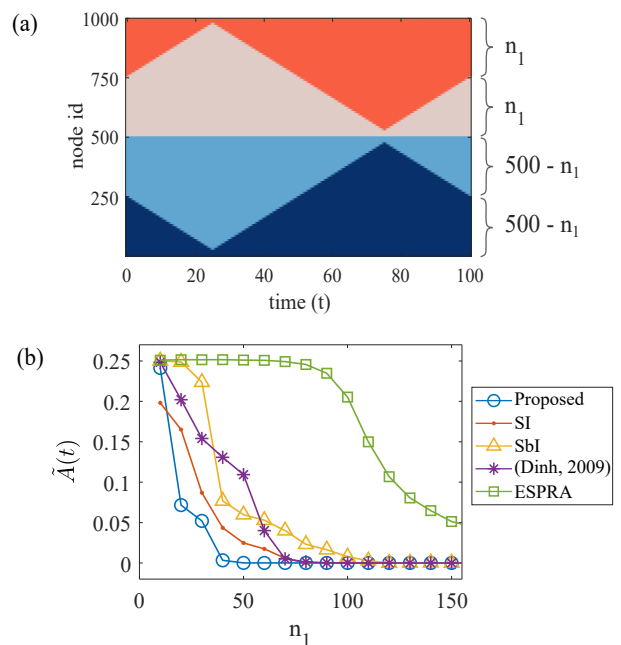


FIG. 6. (a) Planted partitions for a double-stacked version of the grow-shrink benchmark, with  $n_1 = 250$ ,  $f = 0.95$ . (b) Squared error of normalized agreement  $E_{\tilde{A}}$  shown for varying  $n_1$  with  $f = 0.5$ .

(Dinh, 2009) have very similar performance, both having  $E_{\tilde{A}} < 0.01$  for all values of  $f$ . The other algorithms perform significantly worse. To gain further insight into the behavior of the algorithms, we plot the value of  $\tilde{A}(t)$  for each algorithm in Fig. 7(b)-(f). The value of  $f$  is varied along the vertical axis, and the corresponding value of  $\tilde{A}(t)$  is plotted along the horizontal axis as a function of time  $t$ . For the proposed algorithm, (Dinh, 2009), and ESPRA, most errors occur when the communities are most imbalanced (with ESPRA encountering low values of  $\tilde{A}(t)$  over a much wider range of time around these extreme points). SI tends to lose track of the small clusters at  $t = \tau/4$ , resulting in a merge of communities and a sharp drop in agreement. This occurs again at  $t = 3\tau/4$ . SbI fares better due to the more balanced sketches produced by SPIN. Nonetheless, the proposed algorithm exceeds the performance of SbI by maintaining a more balanced sketch once the initial clustering is performed at  $t = 0$ .

### C. Merge-split detection

We now execute the algorithms on the merge-split benchmark. We use two concurrent instances of the merge-split process, such that both instances undergo a split and merge simultaneously. The planted partitions are shown in Fig. 8(a). The parameters of the model are  $q = 2$ ,  $n = N/2$ ,  $p_{\text{in}} = 0.5$ ,  $p_{\text{out}} = 0.05$ ,  $q^- = 2$ , and we set  $n' = 50$  for the proposed algorithm. This results in a

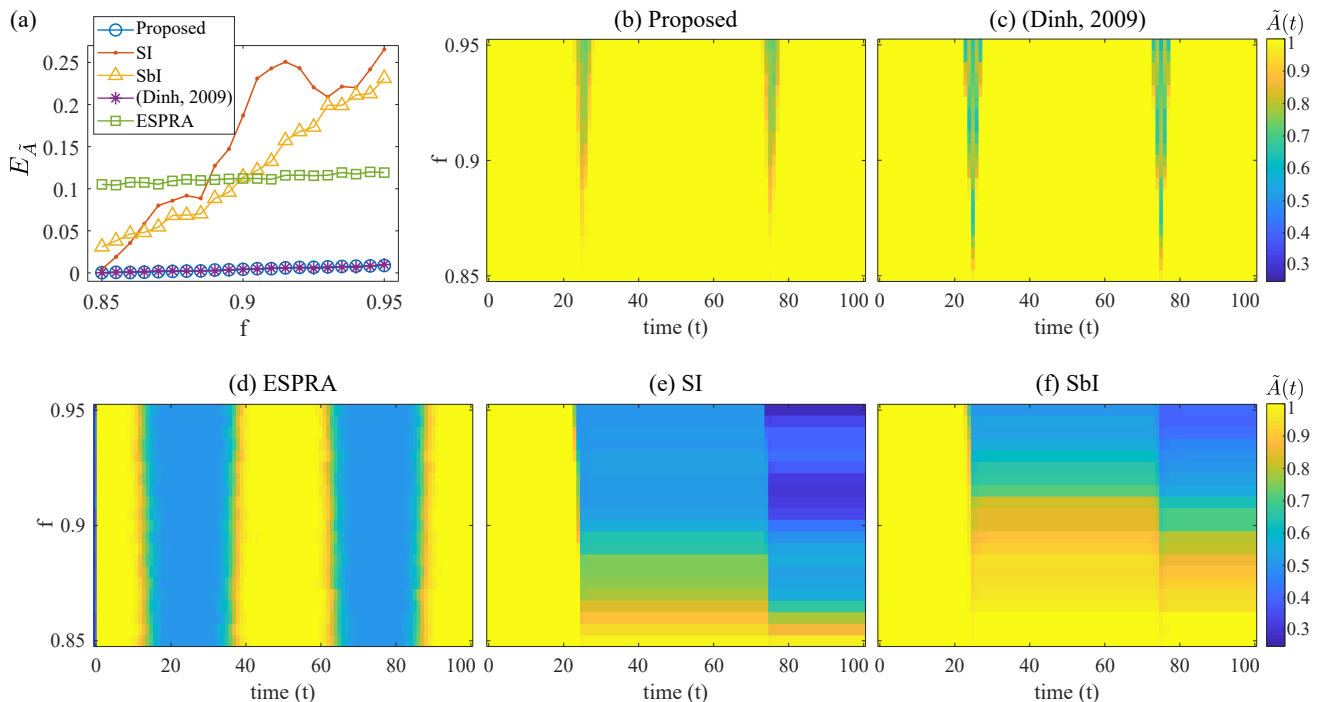


FIG. 7. Results for varying  $f$  in the grow-shrink example in Fig. 6. Plot of  $E_{\tilde{A}}$  is shown in (a). Panels (b) through (f) show heat maps of  $\tilde{A}(t)$  as a function of time along the horizontal axis, and  $f$  along the vertical axis for each algorithm.

sketch size of 100 in the merged state, and 200 in the split state. The partitions reconstructed by the algorithms are shown in Fig. 8(b)-(d).

It is important to note that the network gradually interpolates between the fully merged and fully split states. The planted partitions, on the other hand, undergo an instantaneous transition between these state. This discrepancy means we cannot expect that the estimated partitions will exactly match the planted partitions. Indeed, all three algorithms overestimate the span of time during which the communities are merged. This is as expected since the benchmark defines the instantaneous transition to occur at the theoretical detectability limit.

For the proposed algorithm, nodes start being misclassified at  $t = 19$ . This is expected due to the shrinking density gap  $p_{\text{in}} - p_{\text{inter}}^*$ , as described in Sec. V B. Nonetheless, for the proposed algorithm, the times at which the estimated communities merge and split more closely match the corresponding event times in the benchmark.

#### D. Mixed benchmark

So far, our results have considered individual benchmarks in isolation. We now run the proposed algorithm on the mixed benchmark shown in Fig. 2(a). Recall that this example has concurrent birth-death, grow-shrink and merge-split processes. The network has edge density parameters  $p_{\text{in}} = 0.5$ ,  $p_{\text{out}} = 0.05$ , and minimum number of communities  $q^- = 4$ . The partition estimates

are shown in Fig. 9(a). All of the mismatch occurs in the merge-split communities, which is consistent with our earlier results.

The set of sketches produced by the proposed algorithm is shown in Fig. 9(b). The sketch nodes are sorted vertically according to their planted communities, with their color indicating the estimated community of the corresponding node. The only deviation from the ideal sketch in Fig. 2(b) lies inside the merge-split communities, due to the errors present in the full graph.

The estimated partitions for (Dinh, 2009) are presented in Fig. 9(c). As with the earlier results, (Dinh, 2009) encounters difficulties in correctly identifying the small clusters in the grow-shrink and birth-death communities.

#### E. Effects of sketch size

We now show how the proposed algorithm perform on each benchmark when using different sketch sizes. To best illustrate the effects, we modify the algorithm to only perform tasks relevant to the benchmark being used (details of these modifications will be provided when discussing each result). For this section, we plot the unnormalized agreement [29]

$$A = \frac{1}{N} \max_{\pi} \sum_{\substack{u=1 \\ |C_u| > 0}}^q |C_u \cap \hat{C}_{\pi(u)}|, \quad (27)$$

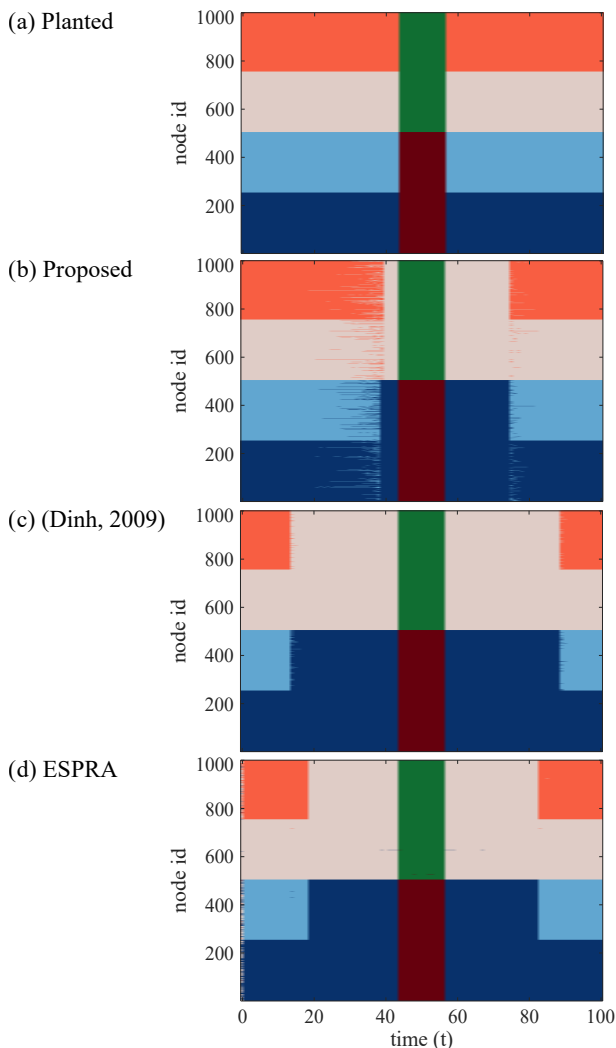


FIG. 8. Planted partitions for a double-stacked version of the merge-split benchmark is shown in (a). Panels (b) through (d) show the estimated partitions for each algorithm.

where  $N$  is the total size of the graph. The agreement for the snapshot at time  $t$  is denoted  $A(t)$ . We plot an ensemble average over 50 independent runs.

Figure 10(a) shows results for the birth-death benchmark example of Fig. 5(a) with  $\gamma=0.15$ . When running the proposed algorithm, we remove steps 19-34. Furthermore, step 7 is changed to  $C_u \leftarrow C'_u(t-1)$ , and step 15 is modified to only iterate over nodes  $i \in V^+(t) \setminus V_{\text{birth}}$ . These changes ensure that only new nodes are assigned a community; existing nodes are left as-is and the merge-split detection is disabled. Recall that  $n'$  is the number of nodes included in the sketch from each community. As  $n'$  increases, the estimate in step 15 becomes more reliable as the variance of  $s_{i,u}(t)$  falls [see (16)]. When  $n' = 10$ , the initial clustering has a large number of errors, and new nodes are consistently misclassified, resulting in a steady drop in agreement. For  $n' = 20$ , the initial partitioning is perfect. Nonetheless, the new nodes that are

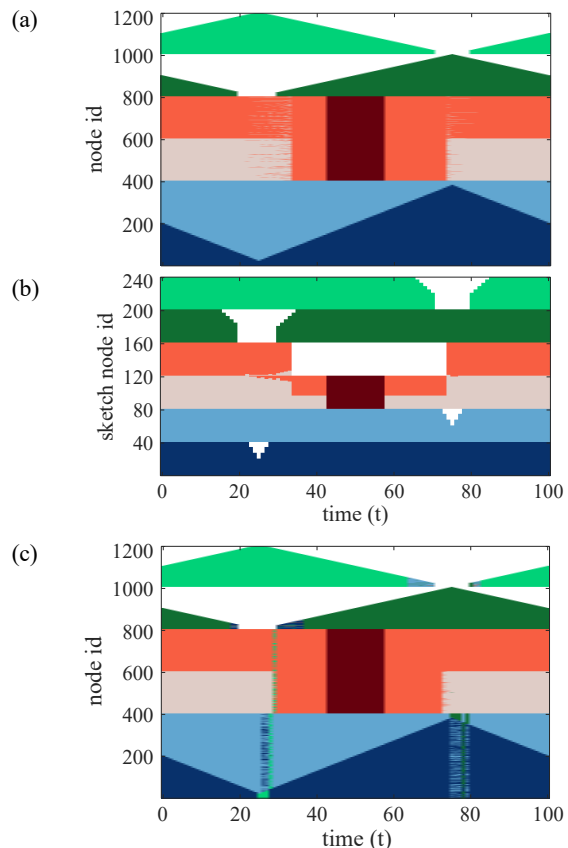


FIG. 9. Results for mixed benchmark. Estimated partitions produced by the proposed algorithm are shown for (a) the full network and (b) the sketches produced by the proposed algorithm. The estimated partitions produced by (Dinh, 2009) are shown in (c).

added after the first birth event are still consistently misclassified. When  $n' = 40$  the reconstructed partitions are almost exactly correct, with  $A(t) > 0.997$  for all time steps.

In Fig. 10(b), we show the results for the grow-shrink example of Fig. 6(a) with  $f=0.95$ . We modify the proposed algorithm by removing steps 19-34 such that the algorithm only re-clusters individual nodes, without merging or splitting communities. For  $n' = 20$ , a large number of misclassifications occur around the extreme points when the community sizes are most imbalanced at  $t = \tau/4$  and  $t = 3\tau/4$ . This occurs for the same reason as the misclassifications in the birth-death benchmark. As expected, as  $n'$  increases, the misclassification rate drops.

In Fig. 10(c), we show results for the merge-split benchmark shown in Fig. 8(a). We modify the proposed algorithm by removing steps 8-14, and changing step 7 to  $C_u \leftarrow C'_u(t-1)$ , such that only merges and splits can occur, and preventing individual nodes from being reclassified. For  $n' = 25$ , the estimates  $\hat{p}_{\text{in}}$  and  $\hat{p}_{\alpha,\alpha'}$  used in step 30 become less reliable. This leads to more variation in the merge detection, as evidenced by the smoothed

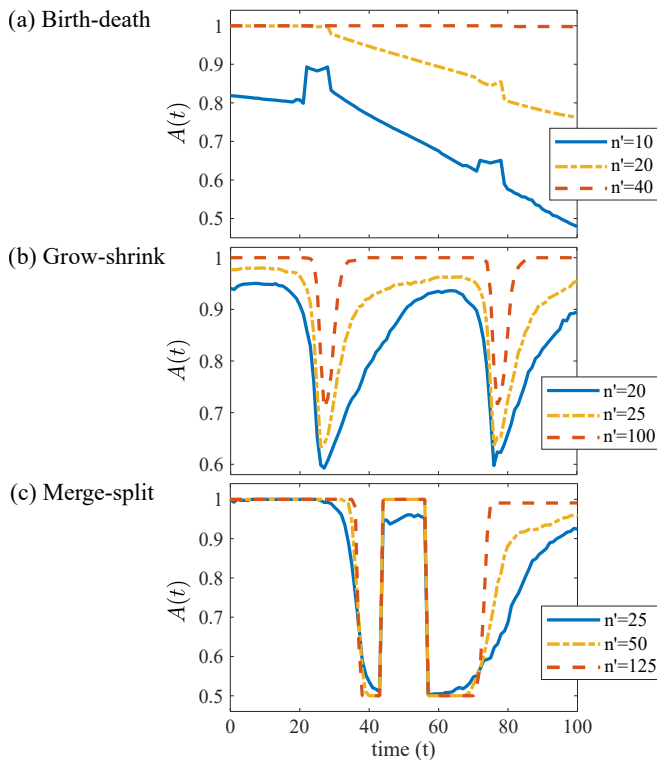


FIG. 10. Effects of varying sketch size for each benchmark.

transition in the value of  $A(t)$  (which is averaged over multiple runs). Similarly, the estimate of the eigenvalues used in step 23 are also less reliable, leading to similar variability in the split detection. As  $n'$  increases,

the merge and split events become more consistent, thus leading to a sharp transition for  $n' = 125$ . Note that for reasons described in Sec. VIC, there is a consistent misclassification of roughly half of the communities for  $38 \leq t \leq 43$  and  $57 \leq t \leq 70$ .

## VII. CONCLUSION

We have presented a sketch-based approach for community detection in time-evolving networks. We presented techniques for handling two existing fundamental processes: one involving growing and shrinking communities, and the other involving merging and splitting communities. We presented a third fundamental process involving the birth and death of communities, as well as techniques to handle these events. An algorithm was presented incorporating these techniques to handle concurrent processes.

Our approach is extendable to other graphs as well, for example the Degree Corrected SBM (DCSBM) [30]. This can be accomplished by substituting a suitable sampling technique for constructing DCSBM sketches, a new similarity definition between each node and the sketch communities, and an appropriate technique for determining whether clusters split or merge.

## ACKNOWLEDGMENTS

This work was supported by NSF CAREER Award CCF-1552497. The University of Central Florida Advanced Research Computing Center provided computational resources that contributed to results reported herein.

- 
- [1] C. Aggarwal and K. Subbian, *ACM Comput. Surv.* **47**, 10:1 (2014).
  - [2] D. Greene, D. Doyle, and P. Cunningham, in *2010 International Conference on Advances in Social Networks Analysis and Mining* (2010) pp. 176–183.
  - [3] G. Cormode, M. Garofalakis, P. J. Haas, and C. Jermaine, *Foundations and Trends in Databases* **4**, 1 (2011).
  - [4] M. Rahmani, A. Beckus, A. Karimian, and G. K. Atia, *IEEE Transactions on Signal Processing* **68**, 962 (2020).
  - [5] A. Beckus and G. K. Atia, in *Proc. IEEE 29th Int. Workshop Mach. Learn. Signal Process* (2019) pp. 1–6.
  - [6] A. Clauset, M. E. J. Newman, and C. Moore, *Phys. Rev. E* **70** (2004), art. no. 066111.
  - [7] N. Dakiche, F. B.-S. Tayeb, Y. Slimani, and K. Benatchba, *Inform. Process. Manag.* **56**, 1084 (2019).
  - [8] S. Zhang and H. Zhao, *Phys. Rev. E* **85**, 066114 (2012).
  - [9] J. Shang, L. Liu, X. Li, F. Xie, and C. Wu, *Physica A* **443**, 70 (2016).
  - [10] C. Granell, R. K. Darst, A. Arenas, S. Fortunato, and S. Gómez, *Phys. Rev. E* **92**, 012805 (2015).
  - [11] P. W. Holland, K. B. Laskey, and S. Leinhardt, *Soc. Netw.* **5**, 109 (1983).
  - [12] G. Rossetti and R. Cazabet, *ACM Comput. Surv.* **51**, 35:1 (2018).
  - [13] J. Hopcroft, O. Khan, B. Kulis, and B. Selman, *P. Natl. Acad. Sci.* **101**, 5249 (2004).
  - [14] T. N. Dinh, Ying Xuan, and M. T. Thai, in *IEEE IPCCC* (2009) pp. 161–168.
  - [15] V. D. Blondel, J.-L. Guillaume, R. Lambiotte, and E. Lefebvre, *J. Stat. Mech.* **2008**, P10008 (2008).
  - [16] J. He and D. Chen, *Physica A* **429**, 87 (2015).
  - [17] T. Yang, Y. Chi, S. Zhu, Y. Gong, and R. Jin, *Mach. Learn.* **82**, 157 (2011).
  - [18] A. Ghasemian, P. Zhang, A. Clauset, C. Moore, and L. Peel, *Phys. Rev. X* **6**, 031005 (2016).
  - [19] K. S. Xu and A. O. Hero, *IEEE J. Sel. Topics Signal Process* **8**, 552 (2014).
  - [20] C. Matias and V. Miele, *J. R. Stat. Soc. B* **79**, 1119 (2017).
  - [21] M. Pensky and T. Zhang, *Electron. J. Statist.* **13**, 678 (2019).
  - [22] A. Decelle, F. Krzakala, C. Moore, and L. Zdeborová, *Phys. Rev. Lett.* **107**, 065701 (2011).
  - [23] U. Von Luxburg, *Stat. Comput.* **17**, 395 (2007).
  - [24] A. Y. Ng, M. I. Jordan, and Y. Weiss, in *Advances in Neural Information Processing Systems*, edited by T. G.

- Dietterich, S. Becker, and Z. Ghahramani (MIT Press, 2002) pp. 849–856.
- [25] A. R. Benson, D. F. Gleich, and J. Leskovec, *Science* **353**, 163 (2016).
- [26] T. Aynaud, E. Fleury, J.-L. Guillaume, and Q. Wang, Communities in evolving networks: Definitions, detection, and analysis techniques, in *Dynamics On and Of Complex Networks, Vol. 2* (Springer, 2013) pp. 159–200.
- [27] P. Jaccard, *New Phytologist* **11**, 37 (1912).
- [28] P. Wang, L. Gao, and X. Ma, *Journal of Statistical Mechanics: Theory and Experiment* **2017**, 013401 (2017).
- [29] E. Abbe, *Found. Trends. Commun. Inform. Theor.* **14**, 1 (2018).
- [30] B. Karrer and M. E. J. Newman, *Phys. Rev. E* **83**, 016107 (2011).